AGU PUBLICATIONS

Geophysical Research Letters

RESEARCH LETTER
10.1002/2017GL072954

Special Section:
Early Results: Juno at Jupiter

Infrared observations of Jovian aurora from Juno's first orbits: Main oval and satellite footprints

A. Mura[1], A. Adriani[1], F. Altieri[1], J. E. P. Connerney[2], S. J. Bolton[3], M. L. Moriconi[4], J.-C. Gérard[5], W. S. Kurth[6], B. M. Dinelli[4], F. Fabiano[1,4], F. Tosi[1], S. K. Atreya[7], F. Bagenal[8], G. R. Gladstone[3], C. Hansen[9], S. M. Levin[10], B. H. Mauk[11], D. J. McComas[12], G. Sindoni[1], G. Filacchione[1], A. Migliorini[1], D. Grassi[1], G. Piccioni[1], R. Noschese[1], A. Cicchetti[1], D. Turrini[1,13], S. Stefani[1], M. Amoroso[14], and A. Olivieri[14]

[1]INAF-Istituto di Astrofisica e Planetologia Spaziali, Rome, Italy, [2]NASA Goddard Space Flight Center, Greenbelt, Maryland, USA, [3]Southwest Research Institute, San Antonio, Texas, USA, [4]CNR-Istituto di Scienze dell'Atmosfera e del Clima, Bologna, Italy, [5]LPAP, Université de Liège, Liège, Belgium, [6]Department of Physics and Astronomy, University of Iowa, Iowa City, Iowa, USA, [7]Department of Atmospheric, Oceanic, and Space Sciences, University of Michigan, Ann Arbor, Michigan, USA, [8]Laboratory for Atmospheric and Space Physics, University of Colorado Boulder, Boulder, Colorado, USA, [9]Planetary Science Institute, Tucson, Arizona, USA, [10]Jet Propulsion Laboratory, California Institute of Technology, Pasadena, California, USA, [11]The Johns Hopkins University Applied Physics Laboratory, Laurel, Maryland, USA, [12]PPPL, Princeton University, Princeton, New Jersey, USA, [13]UDA, Departamento de Fisica, Universidad de Atacama, Copiapó, Chile, [14]Agenzia Spaziale Italiana, Rome, Italy

Key Points:
- Detailed observation of a very long tail of the Io magnetic footprint
- Identification of thin multiple arc structures in the northern and southern ovals, and of bright spots and depletion in the south pole
- Filamentation of alternatively upward and downward current in the 0°–90° SIII sector in the north

Correspondence to:
A. Mura,
alessandro.mura@inaf.it

Citation:
Mura, A., et al. (2017), Infrared observations of Jovian aurora from Juno's first orbits: Main oval and satellite footprints, *Geophys. Res. Lett.*, *44*, 5308–5316, doi:10.1002/2017GL072954.

Received 5 FEB 2017
Accepted 5 MAY 2017
Accepted article online 25 MAY 2017
Published online 3 JUN 2017

Abstract The Jovian Infrared Auroral Mapper (JIRAM) is an imager/spectrometer on board NASA/Juno mission for the study of the Jovian aurorae. The first results of JIRAM's imager channel observations of the H_3^+ infrared emission, collected around the first Juno perijove, provide excellent spatial and temporal distribution of the Jovian aurorae, and show the morphology of the main ovals, the polar regions, and the footprints of Io, Europa and Ganymede. The extended Io "tail" persists for ~3 h after the passage of the satellite flux tube. Multi-arc structures of varied spatial extent appear in both main auroral ovals. Inside the main ovals, intense, localized emissions are observed. In the southern aurora, an evident circular region of strong depletion of H_3^+ emissions is partially surrounded by an intense emission arc. The southern aurora is brighter than the north one in these observations. Similar, probably conjugate emission patterns are distinguishable in both polar regions.

1. Introduction

The Jovian Infrared Auroral Mapper (JIRAM) [*Adriani et al.*, 2008, 2014, 2016] is an imaging spectrometer on board the Juno spacecraft, which started the prime mission around Jupiter in August 2016 [*Bolton et al.*, 2017].

The JIRAM investigation was purposely designed to explore the Jovian aurorae and the planet's atmospheric structure, dynamics, and composition. The main auroral oval emission is thought to be associated with upward field-aligned currents driven by the breakdown of corotation between the planet and the plasma sheet, partially supplied as neutral gas by Io's volcanic activity. It has been suggested that such breakdown occurs at equatorial magnetospheric distances from 15 to 40 RJ and generates a global current system whose upward branch is associated with auroral precipitation [*Cowley and Bunce*, 2001; *Hill*, 2001]. Outside of the main oval, signatures of electromagnetic interactions between Jupiter and its moons (particularly Io) are present [*Connerney et al.*, 1993]. These signatures, known as *footprints*, are produced as the moon crosses and perturbs the equatorial plasma flow [*Saur et al.*, 1999] and Alfvén waves propagate from the satellite position along the magnetic field lines toward the planet.

Emissions poleward of the main auroral oval are thought be connected to the outer magnetosphere, possibly related to a sector of the Dungey and Vasyliûnas cycle flows [*Cowley et al.*, 2003; *Grodent et al.*, 2003]. In the UV, this region shows the highest temporal and spatial variability and this is where the largest differences in comparison to IR emission behaviors have been observed [*Radioti et al.*, 2013; *Stallard et al.*, 2016].

Emission due to the H_3^+ ion is prominently observable in the JIRAM spectral range. Its main roto-vibrational band is around 2521 cm^{-1}, composed of more than 200 possible transitions in the range 3.0–5.0 μm; observation of the infrared emission of H_3^+ is mainly possible in a spectral interval (3.2 to 4.0 μm) where the solar and thermal radiance emitted by the planet are very low due to the intense atmospheric methane absorption

band, resulting in a high auroral contrast against Jupiter's dark disk [*Connerney and Satoh*, 2000]. H_3^+ is the result of H_2^+ ionization (by energetic electrons) and reaction with neutral H_2:$H_2^+ + H_2 \rightarrow H_3^+ + H$; excited H_3^+ decays with lifetime of the order of ~15 min [*Stallard et al*., 2002], thus producing the observed IR emission. The H_3^+ is almost in thermal equilibrium with the neutral atmosphere [*Tao et al*., 2011], and the spectrum of the emission depends on the local temperature [*Stallard et al*., 2002]. Hence, infrared observations of Jupiter aurorae, more than being an instantaneous picture of the particle precipitation process as they are in the UV, also monitor the H_3^+ column density and temperature. Together with JIRAM, Juno mission carries an UV auroral spectrograph (UVS, Ultraviolet Spectrograph [*Gladstone et al*., 2014]), to allow comparison of simultaneous observations of both IR and UV emissions from the same regions. JIRAM-UVS comparison, to be performed in future studies, will give more insights on the auroral processes, allowing studies that are not possible by analyzing IR or UV data alone.

2. Data Set

JIRAM combines two data channels (images and spectra) in one instrument. The optical design uses a reflecting telescope and a grating spectrometer in Littrow configuration. Two distinct focal plane detectors are used for imaging and spectroscopy. The aberrations in the telescope and spectrograph optical path are corrected with dioptric doublets. The instrument uses a dedicated despinning mirror to compensate for spacecraft rotation (1 or 2 rotations per minute). The instrument is designed to perform one acquisition, consisting of two 2-D images in different spectral ranges/channels, and a 1-D slit with full spectral resolution, every spacecraft rotation (currently 30 s). JIRAM can tilt its field of view (FoV) above or below the subspacecraft point, along the plane perpendicular to Juno spin axis, by delaying or anticipating the acquisition, which by default is taken at nadir. JIRAM cannot articulate its FoV in any other direction without turning the spacecraft.

The imager channel is a single detector (266 × 432 pixels) with two different filters (128 × 432 px each), separated by a 10 pixel wide, inactive strip. Of the two filters, one (*L* band, from 3.3 to 3.6 μm) is devoted to imaging H_3^+ emission and provides spatial context for the spectral observations. The angular resolution is 0.01°/pixel. The FoV of the *L* band is 5.87° by 1.74°. The spatial resolution, at the surface, varies with the spacecraft radial distance, and it is of the order of 100 km/pixel during most imaging activities. The other filter (*M* band, from 4.5 to 5 μm) is suitable for mapping the thermal structures of the atmosphere. In 2016, prior to orbit insertion, JIRAM observed Jupiter, Io, Europa, Ganymede (from a distance of about 80 million kilometers), and Aldebaran, and a general calibration campaign was performed, including an assessment of pointing precision/accuracy and detector sensitivity. The campaign resulted in minor corrections of the pointing knowledge and of the imager responsivity. This latter was revised to 2×10^6 counts s^{-1}/ (W m^{-2} sr^{-1}) for both the *L* and *M* filters, by comparing the signal detected by the spectrometer (integrated over the *L* or *M* passbands) with the signal detected by the imager filter, for the same target.

JIRAM took more than 4000 images and spectra [*Adriani et al*., 2017; *Dinelli et al*., 2017] of Jupiter's aurorae and atmosphere prior to and immediately following the first Juno perijove pass (27 August 2016). In particular, more than 600 images of the filter-integrated radiance in the *L* band have been collected over the northern and southern aurorae, with an unprecedented spatial resolution and vantage point.

The JIRAM FoV is not able to cover the entire polar region in a single image during Juno's passage over the poles because the spacecraft is too close to Jupiter. However, JIRAM's field of view can be articulated with the scanning mirror to scan across most of the auroral features. These "tilted" images are organized in groups ("scans") of ~25 images each. Each image is a 1 s integration; images are acquired 30 s apart so that a complete scan takes ~12 min to be performed. The resulting mosaic gives a comprehensive image of the aurora and satellite footprints visible within the imaged area. Mosaics are assembled by processing the data to remove contamination (see section 3) and averaging the best available imagery where images overlap.

The northern aurora was observed from 08:24 to 11:51 UTC on 27 August 2016, with a total of 13 scans (one scan was incomplete due to partial data loss). The spatial resolution of these images varies from ~90 down to ~20 km/pixel. The southern aurora was observed from 15:06 to 19:51 UTC on 27 August

2016, with a total of 10 scans acquired. The spatial resolution of these images varies from ~50 to ~130 km/pixel.

3. Data Processing

In some particular cases, the JIRAM *L* band images evidence significant contamination arising from strong signals present in the companion *M* band detector. The origin of the problem is not known at present but remains under study. Possible explanations include stray light within the optical system and/or electron leakage on the detector. This effect is relevant only for the *L* band detector, and it is observed only when the *M* band detector (which is beneath the *L* band one) receives a strong signal from Jupiter in its field of view (Figure 1). The most unfavorable configuration occurs when looking JIRAM images the northern pole: in this case Jupiter fills the *M* band imager field of view. The intensity of the interference is higher than the radiance from H_3^+ emission, and it is therefore necessary to correct the data.

By analyzing the intensity and spatial variation of the interference observed when no real signal is present in the *L* band image FOV, it appears that the contamination is less intense for pixels that are distant from the *M/L* band border. The spatial variation of the interference signal has been fit with an exponential function with three free parameters:

$$N = C\, e^{-x/\lambda} + D \tag{1}$$

where *N* is the noise count rate, *C* is an intensity value, λ is a scale length, *D* is a constant background value, and *x* is the distance, in pixels, from the *L/M* band border along the detector column. For each acquisition, and for each column of the image matrix, parameters *C* and *D* are variable. In contrast, the scale length is found to be almost constant in time and uniform along columns, with a value of about 20; but it too can be slightly tuned to improve the performance of the noise-removal algorithm. In principle, *C* is likely related to the intensity of the signal that is present in the *M* band channel. However, during scientific operations at Jupiter, JIRAM never takes both *M* and *L* images at the same time. Hence, a different approach is taken to find *C* and remove the constant background signal. We subtract the count rates of pixels in a subsequent image viewing the same surface location, and we assume that the signal has not changed between acquisitions 30 s apart, whereby *D* is canceled and *C* can be obtained from

$$N_1 - N_2 = C\left(e^{-x_1/\lambda} - e^{-x_2/\lambda}\right) \tag{2}$$

This also assumes, as a necessary approximation, that *C* is constant in the same column on two subsequent images.

At the end of the procedure the background *D* is still not evaluated, but it is usually less than $\sim 5 \cdot 10^{-5}$ W m^{-2} sr^{-1} and does not significantly affect the data, since the instrument noise equivalent radiance (NER) is 10^{-5} W m^{-2} sr^{-1}. In addition, before every science image acquisition, JIRAM performs a "background frame" acquisition in the antinadir direction (dark sky image) and subtracts that from the targeted science image. This also allows removal of the focal plane's dark current generated by the spurious accumulation of thermal electrons, and the thermal emission generated by the instrument's inner walls and components.

In this way, it is possible to determine the parameters characterizing the noise contribution and partially remove the interference from the *L* band images (primarily northern aurora). The residual noise and some artifacts arising from the noise removal procedure are still visible in Figure 4, but they do not affect the scientific interpretation of the data. We expect that turning off the JPEG compression currently employed to minimize telemetry resource usage will help in removing contamination from the data, because some artifacts are introduced by the JPEG compression as well, and not included in the corrections implemented with equation (2). No other correction has been done to the data to derive the images presented in this study (Figures 2–4).

The measured radiance is mapped onto a reference surface 500 km above the 1 bar level using SPICE/NAIF routines and ancillary data [*Acton*, 1996]. We chose this level as an average altitude, assuming most of the auroral emission originates in the vicinity [*Grodent et al.*, 2001; *Hiraki and Tao*, 2008]. The accuracy of the mapping to 500 km altitude is about as good as the projected pixel size (from 20 to 130 km, see above).

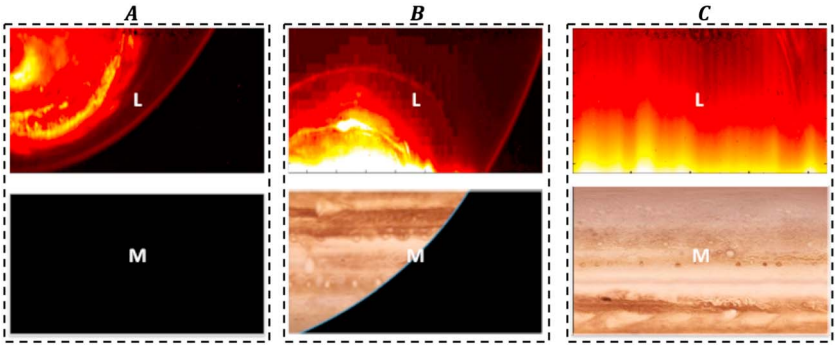

Figure 1. Examples of *L* band data and contamination (top) function of M channel pointing (bottom, graphic art). (a) South Aurora, very low contamination, *M* band FoV is pointing toward empty space. (b) South Aurora, medium contamination in the bottom of the image; *M* band FoV is partially filled by Jupiter. (c) North Aurora, very high contamination, *M* band FoV is completely filled by Jupiter.

Juno's vantage point is close to the planet, and rapidly evolving along the spacecraft trajectory, so the emission angle also evolves rapidly. A higher emission angle implies a longer column for the emitted radiation. The image intensity is adjusted (multiplied by the cosine of the emission angle), assuming that radiance is constant along such column, to normalize the measured radiance to that coming from a vertical column. This also implies that there is no methane absorption above the H_3^+ emission region; in fact, the spectrometer measurements of the auroral region (made with the same viewing geometry of the imager) show that

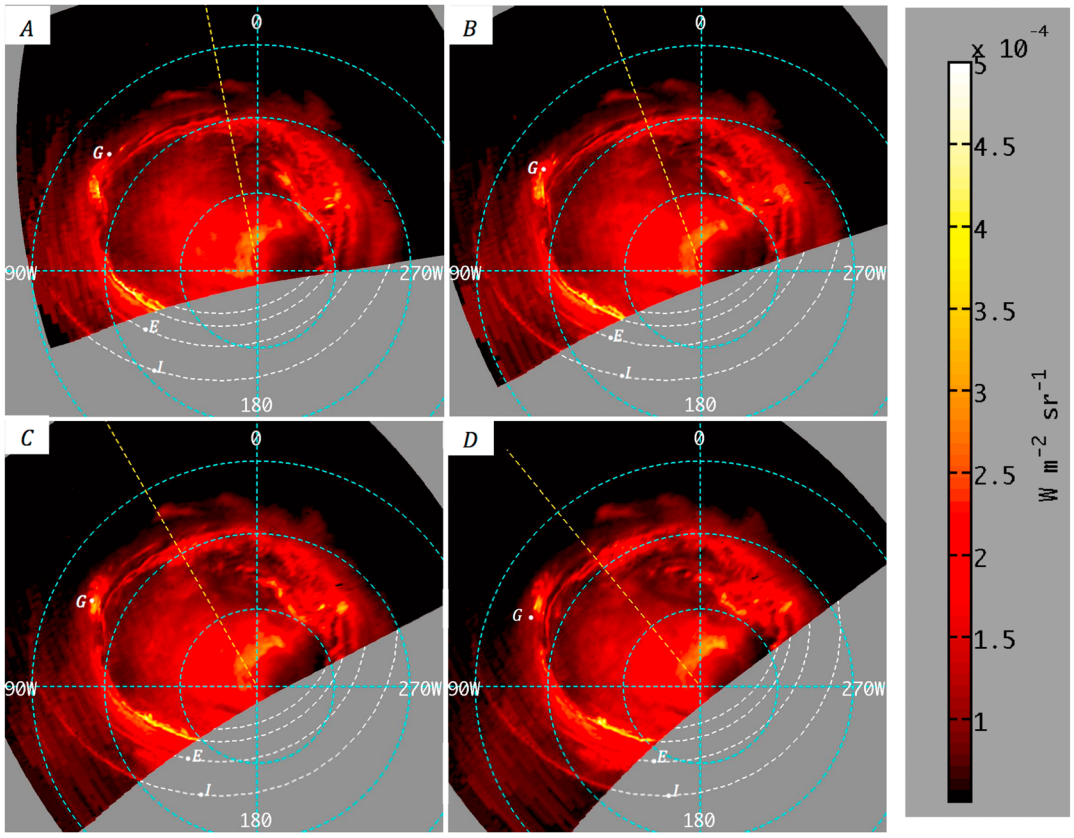

Figure 2. Mosaic maps of emission (3.3–3.6 μm average radiance) from south aurora taken on 27 August 2016. Cyan dashed circles are parallels at 80°, 70°, and 60° latitude; longitudes are SIII; and Sun direction is indicated by yellow line. White dashed lines are footprints of moons and 30 RJ according to VIP4 model (see text for explanations). Starting UTC times of observations are (a) 17:53:59, (b) 18:09:21, (c) 18:24:43, and (d) 18:40:36. White points are predicted footprint positions indicated by letters I, E, and G.

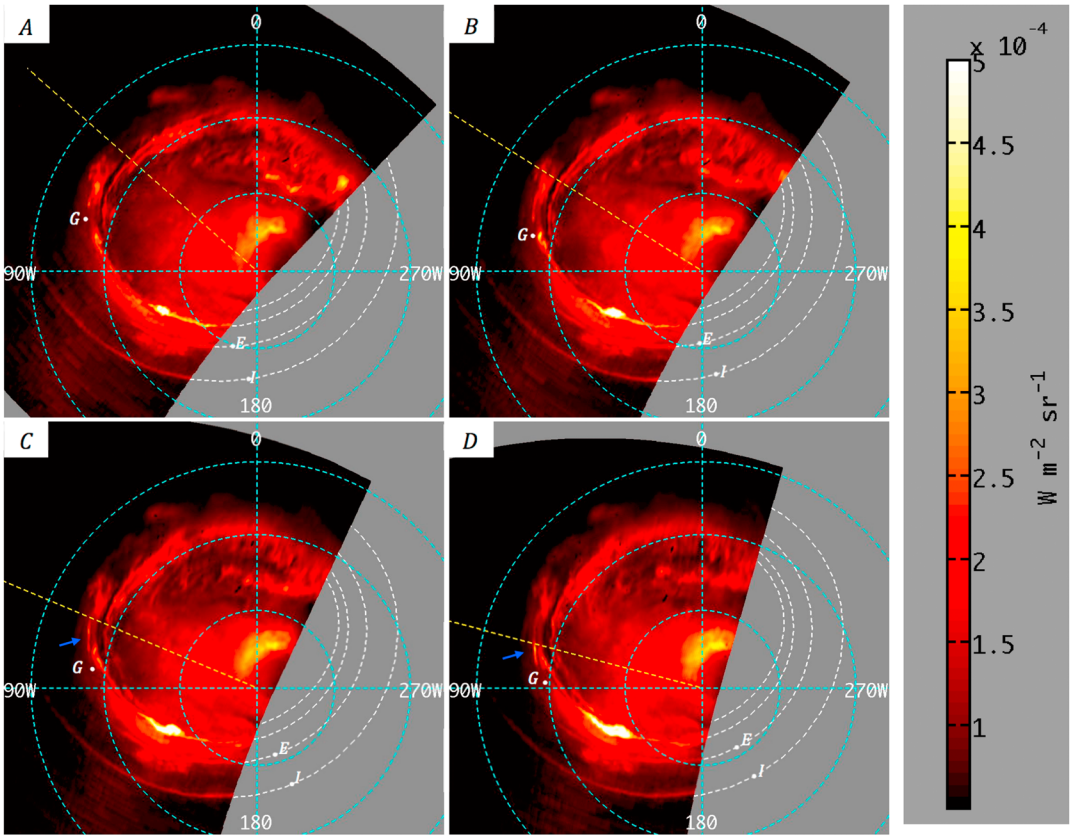

Figure 3. Same as Figure 2, starting UTC times of observations are (a) 18:55:58, (b) 19:11:20, (c) 19:26:42, and (d) 19:41:34. A blue arrow (Figures 3c and 3d only) indicates the feature that is identified as Ganymede footprint.

even where the methane emission is large, it is always superimposed to the H_3^+ spectrum, this indicates that the two molecules either coexist at the same altitudes or the methane layer is below the H_3^+ layer [*Dinelli et al.*, 2017; *Adriani et al.*, 2017; *Moriconi et al.*, 2017]. The image intensity is not the total H_3^+ emission, but only the segment in the filter passband.

4. Satellite Footprints

Io and its ionosphere act as an obstacle for the equatorial plasma flow [*Saur et al.*, 1999]. Alfvén waves propagate from Io's position toward Jupiter along the magnetic field lines, resulting into intense auroral emission [*Connerney et al.*, 1993; *Gérard et al.*, 2006], which is called the Io footprint (FP). Similarly, Europa and Ganymede footprints are generated. Each footprint is hence magnetically connected to the satellite itself, and the study of the location of such footprints gives constraints on the reconstruction of the magnetic field of Jupiter [*Connerney et al.*, 1998]. Each footprint has a main (or multiple main) spot and a tail [*Bonfond et al.*, 2013a, 2013b]. Because of the lifetime of H_3^+ (~15 min), in the case of IR observations such footprints should look like segments of few degrees in the same direction of the "tail."

Figures 2 and 3 show a total of eight mosaic images of south aurora. White dashed lines show (from outside to inside) the magnetic mapping of the orbits of Io, Europa, Ganymede, and 30 Jupiter Radii (as a reference for the main oval) calculated using the VIP4 model [*Connerney et al.*, 1998] combined with a model magnetodisc [*Connerney et al.*, 1981]. The white dots indicate the footprints of the positions of the moons (main spots, also indicated by letters I, E, and G) during the observations according to the same model.

Prints of Io and Europa are very evident in the 90°–180° SIII longitude sector, and the agreement with the VIP4 model footprint locations is so good that we plot the VIP4 reference ovals only outside of the JIRAM image to avoid obscuration of the satellite-related features. Unfortunately, for these images, the instantaneous satellite footprints lie outside of the mapped part of the aurora, and only the trailing tail is visible. In

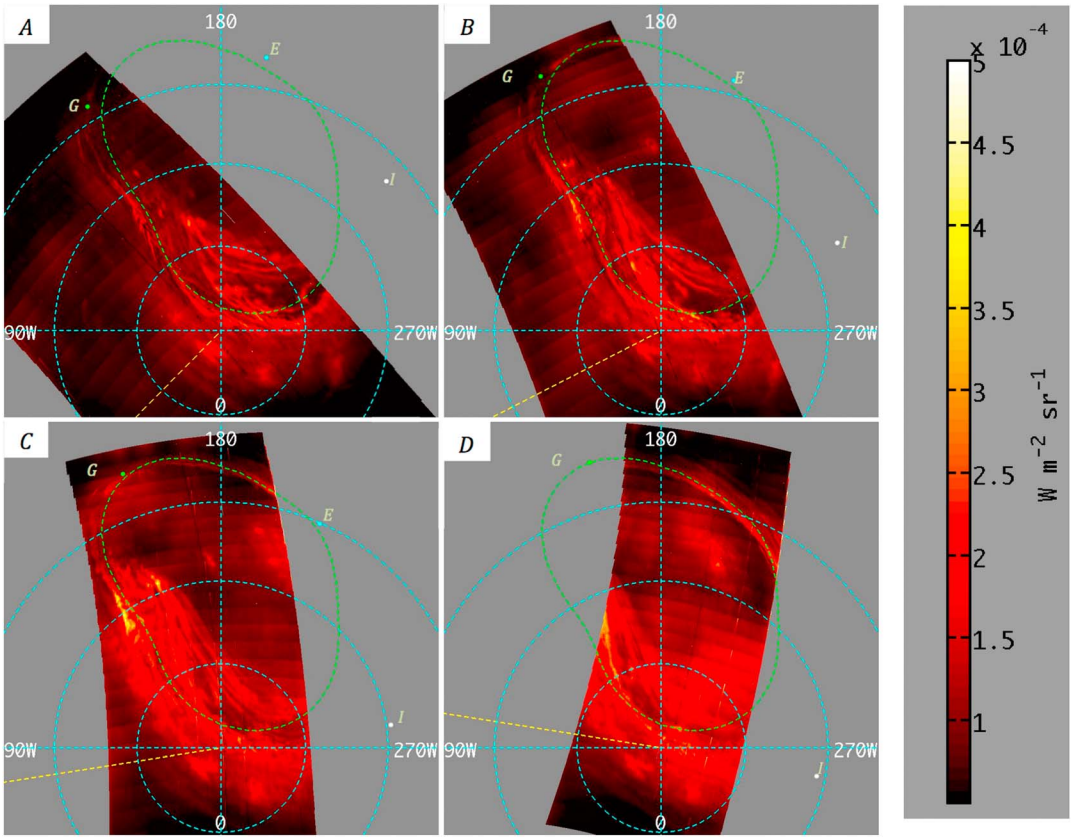

Figure 4. Same as Figure 2, for north aurora. Green dashed line: statistical oval [*Grodent et al.*, 2003]. Green spots are (clockwise) statistical positions of Ganymede, Europa, and Io footprints ([*Hess et al.*, 2011] Europa FP position at the time of Figure 4d was not available). Starting times of observations are (a) 08:53:58, (b) 09:24:11, (c) 09:54:23, and (d) 10:24:05.

the case of Io, the distance between the calculated footprint location and the closest part of the visible tail is ~30° in longitude (~1 h of Jupiter-Io relative rotation). The tail extends for at least 90° in longitude with decreasing intensity but without appreciable change in its thickness (~500 km). The poleward edge is less sharp than the other one, as there is no auroral emission equatorward of the footprint of Io (i.e., no significant particle precipitation originating inside of Io's orbit). The brightness of Io's footprint decreases almost exponentially with a scale of ~2 h (~70°), and it appears that the Io's footprint tail is much longer if observed on unprocessed images (Figure 1b). Similar inferences apply to Europa's footprint; it has a similar intensity as Io's, but it is shorter and, being closer to the main oval, it is observable only for few tens of degrees in longitude. The footprint of Ganymede is visible, and it has two main spots [*Bonfond et al.*, 2013a, 2013b, 2017] ~10° westward of the predicted locations (i.e., above, in the pictures, see the blue arrow in Figures 3c and 3d). It is visible particularly in Figure 3; the two spots are visible in Figures 3a and 3d; in Figure 3c they form a segment and they are undistinguishable. As predicted, each main spot has the shape of a segment of few degrees, approximately in the longitude direction. In Figure 2, it occurs to be too close to a stable, intense emission feature of the main oval, or to an injection signature at lower latitude [*Dumont et al.*, 2014], which covers the footprint. A very faint tail may be present.

Figure 4 shows four mosaic images of north aurora after data processing. The green dashed line is the statistical oval (UV) as in *Grodent et al.* [2003]. The green spots are the expected locations of the Ganymede, Europa, and Io footprints according to the statistical analysis of *Hess et al.* [2011]. None of the main footprint spots are visible in the data; Io and Europa are very far from the FoV, and Ganymede is confused with the main oval emission. For this reason, no footprint model is added to the figure. Only a very tenuous part of the tail of Io may be visible close to 0°E, 80°N, but this feature is attributed to Io only because the positions given by *Hess et al.* [2011] are in correspondence with that feature.

5. Main Oval

Earlier UV observations [*Gérard et al*., 1994; *Ballester et al*., 1996; *Grodent et al*., 2003] show that the shape of the statistical UV main auroral oval is quite repeatable in a Jupiter fixed frame, although second-order variations occur on timescales of tens of minutes, which is comparable to the time resolution of the mosaics (for this reason we prefer not to integrate all data into a single image). Variations include intensifications (~50% increase) of main, stable emission features, and creations, movement, and disappearance of minor structures.

Both in the UV and IR spectral ranges, the Jovian auroral morphology, on a global scale, is very similar and commonly divided into three main components: (1) outer emissions (including the footprints), (2) main oval (or main emission), and (3) polar emissions [e.g., *Satoh and Connerney*, 1999a, 1999b; *Clarke et al*., 2004; *Radioti et al*., 2013]. UV auroral features mainly result from inelastic collisions of energetic electrons of magnetospheric origin with atmospheric molecular hydrogen, whereas IR auroral emissions are due primarily to thermal emissions from the H_3^+ molecular ion at altitudes above the Jovian homopause.

As in UV images [*Grodent et al*., 2003; *Gladstone et al*., 2017; *Connerney et al*., 2017], the main oval (both south and north ones) shows a narrow single arc in about one half of the oval and multiple arcs plus broad diffuse emissions in the other half. However, as Juno's UV and IR images were not obtained at the same instant in time, during this perijove pass, we urge caution in direct comparison of the two. In the infrared, it seems that, in the south, the broad region is between 270° and 0°, and a single arc is visible between 90° and 180° (in Figure 2, smaller arcs are visible stemming from the main one; in Figure 3, i.e., about 1 h later, the single arc turned into a broad region of intense emission; 180°–270° is not covered in the south pole). In the north, a main single arc (plus some parallel secondary arcs) is visible between 150° and 270° (magnetic longitudes), and the broad, multiarc region covers the remaining part. In both hemispheres, the diffuse region shows multiple structures of coherent pattern. The northern aurora, for example, shows concentric arcs of similar morphology (~200 km thick) placed from the main oval poleward, so that one might infer that such features still map to the closed field line region of Jupiter's magnetosphere, as the main oval, even if similar features are not evident in the south (which, however, was observed about 10 h later). These structures, observed in all individual images related to that location, may correspond to a filamentation of alternatively upward and downward current, in contrast to the simple paradigm of a single current loop connecting the magnetosphere and the ionosphere. Part of the remaining region might map to the outer magnetosphere, possibly related to a sector of the Dungey and Vasyliûnas cycle flows [*Cowley et al*., 2003; *Grodent et al*., 2003].

The unprecedented spatial resolution of the JIRAM IR observations helps constrain the thickness of the single arc region, which is found to be uniformly equal to 500 km for the south and 700 km for the north. This could help constraining the theoretical models on the radial velocity distribution, such as that of *Cowley and Bunce* [2001], as in *Grodent et al*. [2003].

The southern aurora appears significantly brighter at the time of observation (~50% higher intensity), as found in the spectrometer measurements [*Adriani et al*., 2017; *Dinelli et al*., 2017]. Three or four diffuse emission spots, placed at 0° System III west longitude and outside the main oval in the south, are visible in the spectrometer data as well and can be linked with similar features in the north aurora at 0° longitude; these may be signatures of plasma injections [*Mauk et al*., 2002; *Dumont et al*., 2014].

6. Summary, Conclusions and Future Perspectives

JIRAM collected ~6 Gb of data before and after PJ1, and the investigation was extremely successful in addressing its primary scientific objectives. In particular, the north and south aurorae have been mapped by both the spectrometer and the *L* band imager channel. High-resolution images of both poles show very thin structures (few hundreds of kilometers) that have the tendency to remain compact within timescales of the order of 1 h. Although the footprints of Europa and Io fell outside the JIRAM FoV in the images acquired in this first periapsis pass, their tails were clearly detected, with a structure both well defined (few hundreds of kilometers width) and extended along the satellite L shell (at least 90° of longitude, probably more). The positions of such tails are in very good agreement with those predicted by the Jupiter magnetic field model of *Connerney et al*. [1998]. The footprint of Ganymede, and possibly its tail, is visible in the southern aurora. The shape of Ganymede main spots, which look like segments of few degrees in the direction of the tail, is consistent with a H_3^+ lifetime of few minutes.

The single arc region of the main oval has a thickness of about 600 km, on average (500 km in the south and 700 km in the north). This parameter is in agreement with predictions, and it can help to constrain theoretical models on the distribution of the equatorial radial velocity of plasma [*Cowley and Bunce*, 2001; *Grodent et al*., 2003].

Inside the main oval, two different types of structures are observed: multiarc structures and bright or dark spots. Multiarc structures appear both in the northern and southern poles. In particular, in the north, such arcs, close to the 0° meridian, are very thin and we interpret these structures, similar in shape to the main oval, as possible signatures of alternatively upward and downward current, in a close field line region.

In the north, inside main oval, small, bright, transient spots are observed with persistence lifetime of hours or less. Outside of the main oval, bright spots are clearly seen close to 0° longitude. There may be signatures of plasma injections [*Mauk et al*., 2002; *Dumont et al*., 2014], and they are substantially stable in a SIII reference.

In the south, a very evident circular region, almost at the pole, shows a strong depletion of H_3^+ emissions. This feature is partially surrounded by a very bright arc, characterized by significant intensity variations.

JIRAM did not collect data on PJ 2 and PJ 3, as a result of the interruption of normal spacecraft operations, but during PJ4 JIRAM returned to normal science operations, to continue spectrometry and imagery of the aurorae.

Acknowledgments
We thank the Italian Space Agency, ASI, for support of the JIRAM contribution to the Juno mission. The JIRAM project has been funded by the Italian Space Agency contract 2016-353 23-H.0. Data in this study will be publicly available on the Planetary Data System (pds.nasa.gov) after the expiration of the data proprietary period.

References

Acton, C. H. (1996), Ancillary data services of NASA's navigation and ancillary information facility, *Planet. Space. Sci.*, *44*(1), 65–70.
Adriani, A., et al. (2008), JIRAM, the image spectrometer in the near infrared on board the Juno mission to Jupiter, *Astrobiology*, *8*(3), 613–622, doi:10.1089/ast.2007.0167.
Adriani, A., et al. (2014), JIRAM, the Jovian infrared Auroral Mapper, *Space Sci. Rev.*, doi:10.1007/s11214-014-0094-y.
Adriani, A., M. L. Moriconi, A. Mura, F. Tosi, G. Sindoni, R. Noschese, A. Cicchetti, and G. Filacchione (2016), Juno's Earth flyby: The Jovian infrared Auroral Mapper preliminary results, *Astrophys. Space Sci.*, *361*(8), 8, doi:10.1007/s10509-016-2842-9.
Adriani, A., et al. (2017), Preliminary results from the JIRAM auroral observations taken during the first Juno orbit: 2—Analysis of the Jupiter southern H_3^+ emissions and comparison with the north aurora, *Geophys. Res. Lett.*, doi:10.1002/2017GL072905, in press.
Ballester, G. E., et al. (1996), Time-resolved observations of Jupiter's far-ultraviolet aurora, *Science*, *274*, 409–412.
Bolton, S. J., et al. (2017), Jupiter's interior and deep atmosphere: The first close polar pass with the Juno spacecraft, *Science*, doi:10.1126/science.aal2108, in press.
Bonfond, B., S. Hess, J.-C. Gérard, D. Grodent, A. Radioti, V. Chantry, J. Saur, S. Jacobsen, and J. T. Clarke (2013a), Evolution of the Io footprint brightness I: Far-UV observations, *Planet. Space Sci.*, *2013*(88), 64.
Bonfond, B., S. Hess, F. Bagenal, J.-C. Gérard, D. Grodent, A. Radioti, J. Gustin, and J. T. Clarke (2013b), The multiple spots of the Ganymede auroral footprint, *Geophys. Res. Lett.*, *40*, 4977, doi:10.1002/grl.50989.
Bonfond, B., D. Grodent, S. V. Badman, J. Saur, J. C. Gérard, and A. Radioti (2017), Similarity of the Jovian satellite footprints: Spots multiplicity and dynamics, *Icarus*, *292*, 208–217.
Clarke, J., D. Grodent, S. Cowley, E. Bunce, P. Zarka, J. Connerney, and T. Satoh (2004), Jupiter's aurora, in *Jupiter: Planet, Satellites, Magnetosphere*, edited by F. Bagenal, T. E. Dowling, and W. B. McKinnon, pp. 639–670, Cambridge Univ. Press, Cambridge, U. K.
Connerney, J. E. P., M. H. Acuna, and N. F. Ness (1981), Modeling the Jovian current sheet and inner magnetosphere, *J. Geophys. Res.*, *86*, 8370–8384, doi:10.1029/JA086iA10p08370.
Connerney, J. E. P., R. Baron, T. Satoh, and T. Owen (1993), Images of excited H_3^+ at the foot of the Io flux tube in Jupiter's atmosphere, *Science*, *262*, 1035–1038.
Connerney, J. E. P., M. H. Acuña, N. F. Ness, and T. Satoh (1998), New models of Jupiter's magnetic field constrained by the Io flux tube footprint, *J. Geophys. Res.*, *103*(A6), 11,929–11,939, doi:10.1029/97JA03726.
Connerney, J. E. P., and T. Satoh (2000), The H_3^+ ion: A remote diagnostic of the Jovian magnetosphere, *Philos. Trans. R. Soc. London, Ser. A*, *358*, 2471–2483.
Connerney, J. E. P., et al. (2017), Jupiter's magnetosphere and aurorae observed by the Juno spacecraft during its first polar orbits, *Science*, doi:10.1126/science.aam5928, in press.
Cowley, S. W. H., and E. J. Bunce (2001), Origin of the main auroral oval in Jupiter's coupled magnetosphere-ionosphere system, *Planet. Space Sci.*, *49*, 1067–1088.
Cowley, S. W. H., E. J. Bunce, T. S. Stallard, and S. Miller (2003), Jupiter's polar ionospheric flows: Theoretical interpretation, *Geophys. Res. Lett.*, *30*(5), 1220, doi:10.1029/2002GL016030.
Dinelli, B. M., et al. (2017), Preliminary results from the JIRAM auroral observations taken during the first Juno orbit: 1—Methodology and analysis applied to the Jovian northern polar region, *Geophys. Res. Lett.*, doi:10.1002/2017GL072929, in press.
Dumont, M., D. Grodent, A. Radioti, B. Bonfond, and J.-C. Gérard (2014), Jupiter's equatorward auroral features: Possible signatures of magnetospheric injections, *J. Geophys. Res. Space Physics*, *119*, 10,068–10,077, doi:10.1002/2014JA020527.
Gérard, J.-C., V. Dols, R. Prange, and F. Paresce (1994), The morphology of the north Jovian ultraviolet aurora observed with the Hubble Space Telescope, *Planet. Space Sci.*, *42*, 905–917.
Gérard, J. C., A. Saglam, D. Grodent, and J. T. Clarke (2006), Morphology of the ultraviolet Io footprint emission and its control by Io's location, *J. Geophys. Res.*, *111*, A04202, doi:10.1029/2005JA011327.
Gladstone, G. R., et al. (2014), The ultraviolet spectrograph on NASA's Juno mission, *Space Sci. Rev.*, doi:10.1007/s11214-014-0040-z.
Gladstone, R., et al (2017), Juno-UVS approach observations of Jupiter's auroras, *Geophys. Res. Lett.*, doi:10.1002/2017GL073377, in press.
Grodent, D., J. H. Waite Jr., and J.-C. Gérard (2001), A self-consistent model of the Jovian auroral thermal structure, *J. Geophys. Res.*, *106*(A7), 12,933–12,952, doi:10.1029/2000JA900129.

Grodent, D., J. T. Clarke, J. Kim, J. H. Waite Jr., and S. W. H. Cowley (2003), Jupiter's main auroral oval observed with HST-STIS, *J. Geophys. Res. Lett.*, *180*(A11), 1389, doi:10.1029/20003JA009921.

Hess, S. L. G., B. Bonfond, P. Zarka, and D. Grodent (2011), Model of the Jovian magnetic field topology constrained by the Io auroral emissions, *J. Geophys. Res.*, *116*, A05217, doi:10.1029/2010JA016262.

Hill, T. W. (2001), The Jovian auroral oval, *J. Geophys. Res.*, *106*, 8101–8107, doi:10.1029/2000JA000302.

Hiraki, Y., and C. Tao (2008), Parameterization of ionization rate by auroral electron precipitation in Jupiter, *Ann. Geophys.*, *26*, 77–86.

Mauk, B. H., J. T. Clarke, D. Grodent, J. H. Waite Jr., C. P. Paranicas, and D. J. Williams (2002), Transient aurora on Jupiter from injections of magnetospheric electrons, *Nature*, *415*, 1003–1005, doi:10.1038/4151003a.

Moriconi, M. L., et al. (2017), Preliminary JIRAM results from Juno polar observations: 3. Evidence of diffuse methane presence in the Jupiter auroral regions, *Geophys. Res. Lett.*, doi:10.1002/2017GL073592, in press.

Radioti, A., M. Lystrup, B. Bonfond, D. Grodent, and J.-C. Gérard (2013), Jupiter's aurora in ultraviolet and infrared: Simultaneous observations with the Hubble Space Telescope and the NASA infrared telescope facility, *J. Geophys. Res*, *118*, 2286–2295, doi:10.1002/jgra.50245.

Satoh, T., and J. E. P. Connerney (1999a), Jupiter's H_3^+ emissions viewed in corrected Jovi magnetic coordinates, *Icarus*, *141*, 236–252.

Satoh, T., and J. E. P. Connerney (1999b), Spatial and temporal variations of Jupiter's H_3^+ emissions deduced from image analysis, *Geophys. Res. Lett.*, *26*, 1789–1792, doi:10.1029/1999GL900372.

Saur, J., F. M. Neubauer, D. F. Strobel, and M. E. Summers (1999), Three-dimensional plasma simulation of Io's interaction with the Io plasma torus: Asymmetric plasma flow, *J. Geophys. Res.*, *104*, 25,105–25,126, doi:10.1029/1999JA900304.

Stallard, T., S. Miller, G. Millward, and R. D. Joseph (2002), On the dynamics of the Jovian ionosphere and thermosphere: II. The measurement of H_+^3 vibrational temperature, column density, and total emission, *Icarus*, *156*, 498–514.

Stallard, T. S., J. T. Clarke, H. Melin, S. Miller, J. D. Nichols, J. O'Donoghue, R. E. Johnson, J. E. P. Connerney, T. Satoh, and M. Perry (2016), Stability within Jupiter's polar auroral 'Swirl region' over moderate timescales, *Icarus*, *268*, 145–155, doi:10.1016/j.icarus.2015.12.044.

Tao, C., S. V. Badman, and M. Fujimoto (2011), UV and IR auroral emission model for the outer planets: Jupiter and Saturn comparison, *Icarus*, *213*, 581–592.